A transverse traveling wave piezoelectric transformer

T Martinez, G Pillonnet, V Loyau, Dejan Vasic, François Costa

A transverse traveling wave piezoelectric transformer

T Martinez[1], G Pillonnet[2], V Loyau[1], D Vasic[1,3] and F Costa[1,4]

[1]Laboratoire SATIE, ENS Paris-Saclay, France
[2]Univ. Grenoble Alpes, CEA, LETI, DACLE, LGECA, Grenoble, France
[3]Université Cergy-Pontoise, Cergy-Pontoise, France
[4]Université Paris-Est, Créteil, France

E-mail: thomas.martinez@satie.ens-cachan.fr

Abstract. Piezoelectric transformers can be a promising candidate in isolated power converters to replace magnetic ones as they present high quality factor, high voltage gain and low electromagnetic compatibility issues. Herein a new topology of *traveling* wave piezoelectric transformer (TWPT) is proposed. Unlike conventional piezoelectric transformers, the proposed transformer uses progressive waves to carry out the electromechanical conversion. The main asset of the structure is the obtaining of a polyphase system of voltage at the output. Thus, associated with an appropriate converter circuit topology, it enables any kind of AC-DC or AC-AC power conversion. The proposed piezoelectric transformer consists in a multi-electrode ring architecture and uses transverse wave, i.e. the deformation is orthogonal to the propagation direction, to perform the electro-mechanical coupling. Furthermore an analytical modelling is exposed to describe the electro-mechanical behaviour of the transformer. The technique allows to obtain an admittance matrix that completely characterizes the coupling between all the electrodes and that can be used to simulate the transformer in electronic circuit software. With this model it is possible to predict numerically the voltages, currents, displacements and stresses in the piezoelectric transformer over time as a function of the geometrical and physical parameters of the materials in early design stage and it allows a co-design between the piezoelectric transformer and its power electronics circuitry. Finally, a prototype of the TWPT with four phase output voltage is presented to experimentally validate this new concept.

1. Introduction

Interest for piezoelectric transformers (PT) increased due to their usefulness power conversions circuits for CCFL backlight applications [1] thanks to their high voltage gain. The CCFL lamps used in this application needed high strike voltage (between 500 and 2000 V) that was difficult to reach for classic magnetic transformer based power converters. However, piezoelectric transformers were already well known in power electronics for their numerous advantages compared to magnetic one: high quality factor that can be greater than 1000 for PZT ceramics, high power density and low electro-magnetic compatibility issues [2]. Furthermore, due to the use of high rigidity dielectric materials, piezoelectric transformers also provide strong galvanic isolation to power converters. Thanks to these different assets, PT can be found in various applications. Their strong electric insulation is used in gate-drive circuits for power-electronics switches [3]. They might also be used in high efficiency resonant DC-DC converters [4]. Their high voltage gain has been used not only in ballast lamp applications but also for high voltage power supply for ozone [5] or plasma generation [6]. Recently they have found an interest in energy harvesting applications. Their high voltage gain

allow for low start-up of thermal-based energy harvester [7,8]. Finally, research is now going in the direction of transformer size reduction by integration of the PT with micro-electronic techniques [9,10]. These foregoing progresses allow for complete integration of power converter and higher working frequencies.

Nevertheless, classic piezoelectric transformers topologies present inherent limits. The working frequency of the PT is fixed by the mechanical and material properties. Furthermore, in conventional piezoelectric transformers, the coupling between primary and secondary sides is realized by mechanical coupling through a *standing wave*. Thus, at their secondary side, there is only one electrode position that will provide a voltage that can be used in power conversion. Other electrode positions would provide lower amplitude voltage (lower coupling) but with the same phase-shift. Finally, all these geometric parameters are set when the design of piezoelectric transformer is carried out and cannot be modified during the power converter application.

However, this issue can be overcome by generating a *traveling wave* instead of a standing wave in the piezoelectric transformer. Whereas a standing wave presents node and anti-nodes that change the output voltage amplitude depending on the electrode position, a traveling wave consists in a waveform that propagates identically alongside the length of the element. In result, the amplitude of all output voltages is the same with a phase-shift between them linked to the wave propagation. In the end, the interest of using a traveling wave in piezoelectric transformers is to obtain a multi-phase output at the secondary side. The use of traveling wave in piezoelectric transformers has already been tackled in [11] but without further deepening on the generation of a multi-phase system.

Traveling wave in piezoelectric elements have already been studied and only used in electromechanical actuator such as ultrasonic motors. For this application, the traveling wave is generated in the stator which generally consists in a piezoelectric ring. Thus a wave propagates in the stator with the deformation orthogonal to the propagation direction that we call a transverse or flexural wave. A rotor located on the stator will then move by friction between the traveling wave in the rotor and the stator [12]. In this application, since it consists in actuation there are no output electrodes and the electrodes only serve the generation of the wave. Several topologies to generate the traveling wave have been proposed [13,14]. In [15], by changing the connection of electrodes, the frequency and thus the speed of the wave can be modified. Integration of those ultrasonic motors have also been proposed in [16] with thin-film deposition techniques. For this application, it is generally necessary to use a traveling flexural wave that will allow the stator to move by friction. However, some ultrasonic motors with different topologies use longitudinal waves [17] or transverse standing waves [18] to create displacement in the rotor. Transverse waves deform the structure orthogonally to the propagation direction as opposed to compression or longitudinal waves that cause deformation in the same direction as the wave motion. Piezoelectric scavengers mainly use transverse wave to harvest mechanical energy [19] and for the generation of the traveling wave in a piezoelectric transformer, both solutions are possible, e.g. longitudinal waves are used in [11].

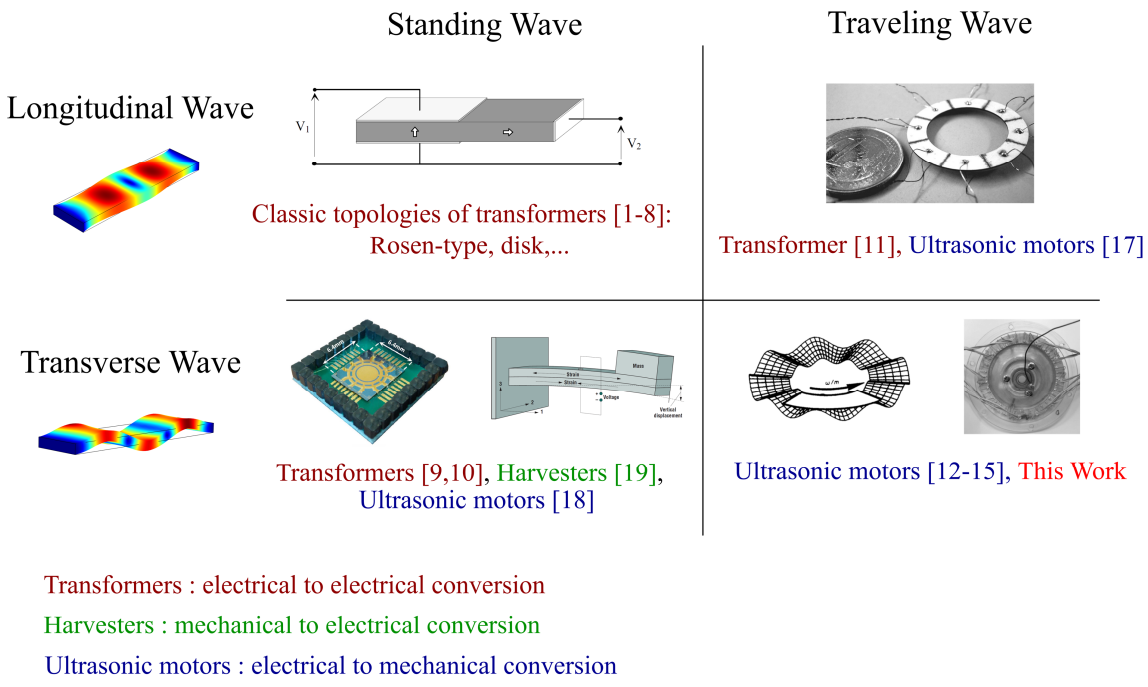

Figure 1. Repartition of the use of piezoelectric systems depending on the type of wave considered

Considering power converters, the interests of obtaining a multi-phase system at the output are numerous. Firstly, it offers more versatility in the type of conversion possible. A traveling wave piezoelectric transformer can be a part of an universal power converter that could realize DC-DC or DC-AC conversion at variable frequency with a polyphase rectifier, a cycloconverter or a matrix converter. Furthermore, with the same principle as interleaved DC-DC converters, increasing the number of phases also increases the apparent working frequency of the system and makes it possible to typically reduce the size of filtering elements without adding extra elements.

In this paper, we propose the case of a traveling wave piezoelectric transformer (TWPT) in power converters. It consists in a ring-type architecture that uses flexural traveling wave to convey the electrical coupling between primary and secondary sides through piezoelectric material. An analytical modelling is proposed to overcome the limits of classic PT modeling adapted to a ring structure and validated by finite element analysis. The modelling results will be validated by experimental measurements obtained with a realized prototype. This paper describes the working principle and design of the TWPT in section 2. The new modeling strategy is then exposed in section 3 and the experimental prototype of the TWPT and results are presented in section 4. Finally in section 5, we focus on the theoretical optimization of the performances of the transformer thanks to the modelling.

2. Structure and working principle of the TWPT

2.1. Choice of the geometry of the TWPT

As contrary to a standing wave, the generation of a traveling wave in a piezoelectric transformer is not obvious. In classic geometries of piezoelectric transformers (Rosen-type, disk), because of the boundary conditions of the mechanical medium, it is difficult to avoid the generation of a standing wave. In the field of ultrasonic motors, where the key function is the generation of the traveling wave, some systems have used straight topologies to generate traveling wave [20]. But in those cases, the system will work outside the resonance of the element. This operation is unacceptable for traveling wave piezoelectric transformers as the aim is to transfer the maximum energy that is only possible close to the resonance.

Other ultrasonic motors topology use ring architecture to generate the traveling wave which will propagate alongside the circumference of the ring. By choosing this topology, we avoid the problem of boundary conditions at the cost of adding complexity to the modelling of the complete system. Moreover, the choice of this topology presents the asset of working at the resonance of the piezoelectric system and allows obtaining the highest energy transfer between primary and secondary sides of the transformer. The geometry of the TWPT is shown in Figure 2. The use of two piezoelectric layers polarized in opposite direction is necessary for flexural wave generation. The piezoelectric layers are polarized in the thickness direction and the voltage applied is applied in the thickness direction. As the piezoelectric mode is the 31 mode, when a positive voltage is applied the upper layer will stretch; as opposite the lower one will compress thus leading to a flexion of the structure.

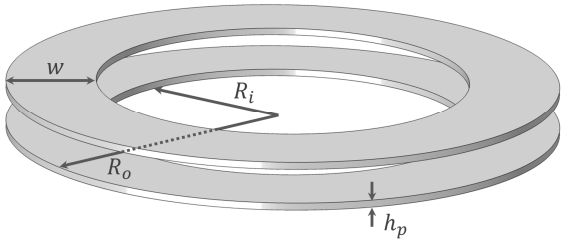

Figure 2. Ring Architecture of the proposed TWPT with the two piezoelectric layers

2.2. Generation of the traveling wave in ring structure at resonant frequency

Although the choice of the geometry is a necessary condition to the generation of the traveling wave, it is not sufficient. If the mechanical structure is excited with a sinusoidal voltage at the resonance frequency, a standing wave appears. To create a traveling wave, a particular excitation scheme is also needed.

We must consider firstly a standing wave represented by the term f in (1). The oscillation pulsation of this wave is ω and its wavelength λ.

$$f(x,t) = U\cos(\omega t)\cos(\frac{2\pi x}{\lambda}) \tag{1}$$

We consider now a second standing wave g with $\frac{\pi}{2}$ phase-shift and a $\frac{\lambda}{4}$ displacement compared to *f*:

$$g(x,t) = U\sin(\omega t)\sin(\frac{2\pi x}{\lambda}) \tag{2}$$

The combination of the two standing waves will lead to the generation of traveling wave:

$$h(x,t) = U\cos(\omega t)\cos\left(\frac{2\pi x}{\lambda}\right) + U\sin(\omega t)\sin\left(\frac{2\pi x}{\lambda}\right) = U\cos\left(\omega t - \frac{2\pi x}{\lambda}\right) \tag{3}$$

The same can applied to the ring geometry of the piezoelectric transformer. The objective will then be to generate the two standing waves f and g in the structure. The excitation of a piezoelectric structure is obtained by application of sinusoidal voltages on the electrodes at the surface of the ring. Two aspects need to be tackled: the $\frac{\lambda}{4}$ displacement and the $\frac{\pi}{2}$ phase-shift between f and g. For the first aspect, it will depend on the electrode scheme at the surface of the ring. Figure 3 a) represents the typical scheme used for the mode 3 of flexural mode. The mode 3 corresponds to the one represented in Figure 4 for which the wavelength is equal to a third of the perimeter of the ring. The electrodes are separated into three groups: electrodes A responsible for the generation of the standing wave f, electrodes B for the standing wave g and output electrodes. In this scheme the electrodes A and B are separated by a distance $\frac{\lambda}{4}$ that creates the displacement between the standing waves. In order to obtain

a traveling wave, the two standing waves must be balanced and thus there is the same number of electrodes A and B. The electrodes in white represent the output electrodes. In this scheme, we can see 8 input and 4 output electrodes. It means that, as the traveling wave will pass alongside the circumference of the ring, we will obtain a four phase system at the output of the TWPT. In theory, it would be possible to obtain a traveling wave with only two input electrodes and the rest as output electrodes as shown in Figure 3 b). However, after flowing over output electrodes, the traveling wave would lose energy and the output voltage at the end would be much lower than the one at the beginning. The use of several input electrodes allows regeneration of the wave at each passage over it and thus regularity in the amplitude of the output voltage. Furthermore, the increase of the number of output electrodes does not mean more phases at the output. As the traveling wave is periodic, we will also obtain four phases. It could be possible anyway to obtain more phases by dividing the output electrodes more as shown in Figure 2 c). In this case, we obtain an octophase system at the output. Finally, the proposed scheme here is valid for this mode of resonance but can be applied to other odd resonance modes especially the fifth one as in Figure 2 d). For even resonance modes, i.e. when the wavelength is an odd fraction of the perimeter, the symmetry of the electrode scheme prevents the generation of the traveling wave.

The second aspect for the generation of the traveling wave is the $\frac{\pi}{2}$ phase-shift. This is achieved by choosing the voltage applied on the electrodes. For the electrodes A, a voltage $V_a = V_{in}\cos(\omega t)$ will be applied whereas for electrodes B we will consider $V_b = V_{in}\sin(\omega t)$.

Finally, the combination of the geometry of the TWPT, the electrode scheme and the choice of excitation voltages allow the generation of the traveling wave. This traveling wave will propagate alongside the circumference of the ring. For an output electrode the output voltage will be then linked to the average stress on its surface and we will obtain sinusoidal voltages at the output at the same pulsation ω. Their amplitude depends on the size of the output electrode as is the number of phases. The more output electrodes at the output, the more different phases we can obtain but the output voltage amplitude is reduced.

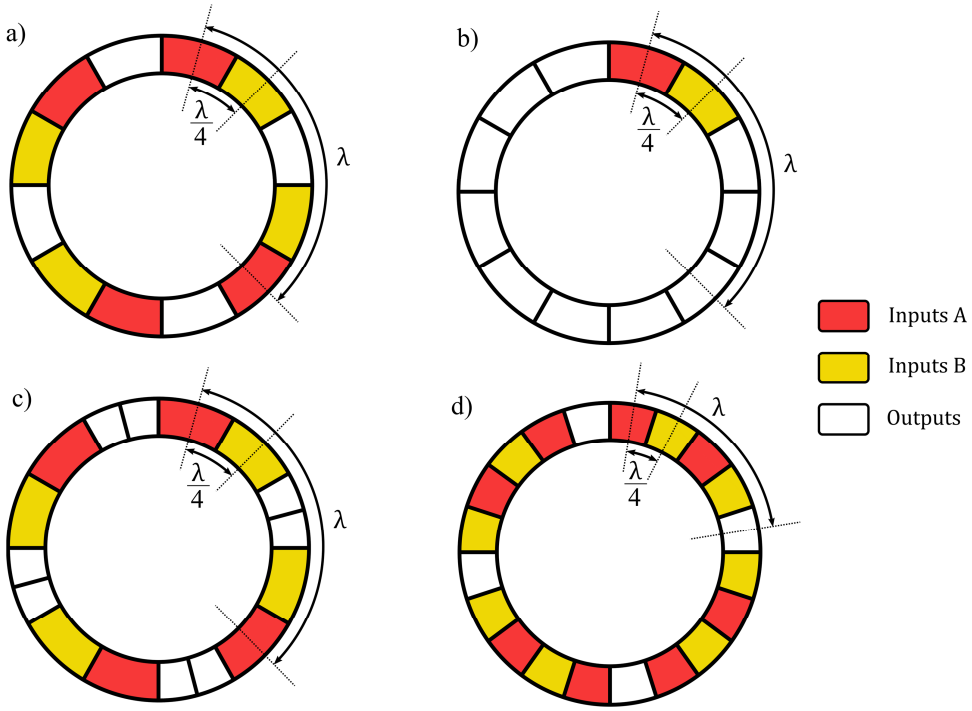

Figure 3. Electrode schemes on the surface of the TWPT for different configuration : a) Mode 3 with 8 input electrodes and 4 output phases b) Mode 3 with 2 input electrodes and 4 output phases c) Mode 3 with 8 input electrodes and 8 output phases d) Mode 5 with 16 input electrodes and 4 output phases.

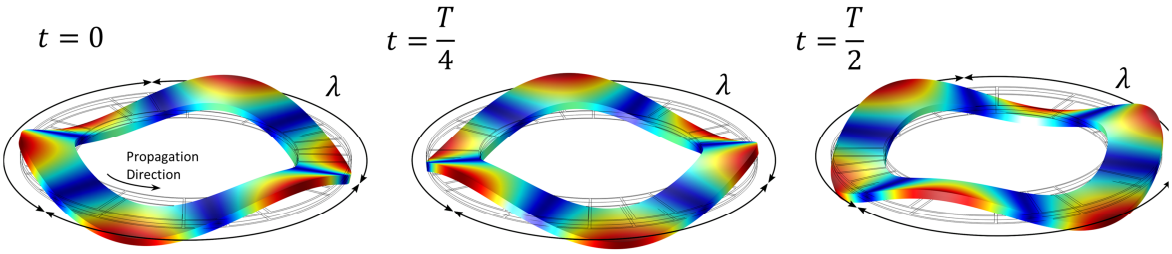

Figure 4. 3rd flexural mode of a piezoelectric ring at different instants of the traveling wave passage

3. Analytical modelling of the TWPT

3.1. Motivations and modelling strategy

The modelling of piezoelectric transformers is a key aspect in the design of power converters. As they are part of complete electrical system, it is necessary to have a compact modelling allowing for fast electrical simulation and co design between the piezoelectric transformer and the circuit. Classical topologies of standing wave PT are well modelled by RLC circuits obtained by mechanical analysis of the structure [21]. However, this modelling is only possible because of the boundary conditions of these topologies. Moreover, most of these architectures use bulk waves that further simplify the modelling. When studying the modelling of traveling waves, we face several issues. The first one concerns thus the boundary conditions. With no boundary conditions in the propagation direction, it appears difficult to simplify mathematically the modelling to a RLC circuit. Furthermore, as seen in

the previous section, the TWPT consists in numerous electrodes that will also have numerous couplings between them. Finally the final aspect is how to take into account and represent the propagation of the traveling wave.

The modelling of traveling wave piezoelectric elements has already been tackled in ultrasonic motors. However, their aim is to obtain an electro-mechanical model that links the amplitude of the deformation to the geometrical and material properties, electrode scheme and voltages applied. By definition the modelling does not have mode electrical coupling between input and output electrodes. Finite element [22] or finite volume [23] analysis can be conducted to characterize the behaviour of the motor. The use of equivalent circuit similar to piezoelectric transformer analysis is possible [24]. Modelling results can also be obtained by using Hamilton's principle applied to Lagrangian representation of the piezoelectric motor [25]. These models are very precise but in this case the complete system is known that is to say the voltage applied at the input and the mechanical constraints at the output, i.e the force applied by the rotor on the stator, and thus the complete external variables can be determined. This method has been applied to the modelling of a Rosen-type piezoelectric transformer [26]. However, when considering a power converter, the load varies along time and can be non-linear making it difficult to use these methods.

Our aim is to obtain a compact modelling of the TWPT that characterizes the coupling between the electrodes and its behaviour before fabrication and that can be simulated in electric simulation software regardless of the load. To do that, we propose to obtain an admittance matrix Y_{tot} linking all the currents to the voltages on all the electrodes of the TWPT. The representation of the TWPT by an admittance matrix is related to the representation of two-port network or in this case multi-port network as shown in Figure 5 a). The same representation is used for the currents and voltages of the TWPT with a bigger number of ports in Figure 5 b). By finding this admittance matrix, the system is completely described. The proposed strategy to get Y_{tot} is based on the modelling of bimorph bridge and beam piezoelectric transformer presented in [27] and consists in separating the ring into sections of ring each corresponding to one electrode. For each section we can then define a chaining matrix that links mechanical variables at one side to the ones at the other side and the voltage. By chaining all the matrices alongside the circumference of the ring, we can obtain in the end the admittance matrix Y_{tot}.

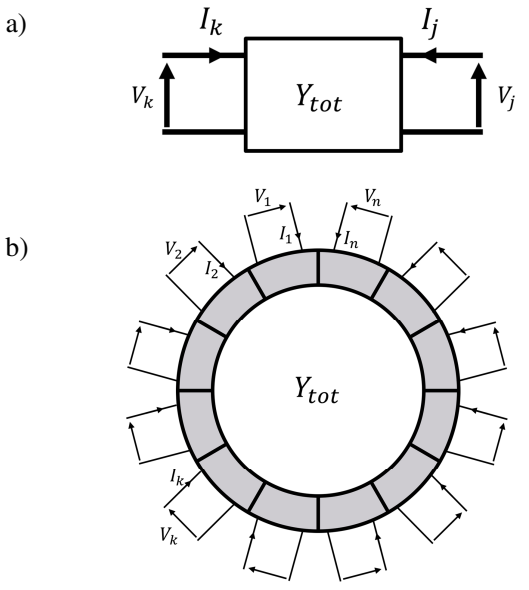

Figure 5. Two-port network representation (a) and ring with n electrodes representation (b)

The main hypothesis made for the modelling is to treat these ring sections as finite beams. The objective of this assumption is to reduce the problem to a one-dimension one with the position along the circumference of the ring as the only variable. With this assumption made, the emphasis is put on complexity reduction of the analysis at the cost of less precision on the absolute results. However, the overall behaviour of the TWPT is still well characterized. Finally, as stated before, the ring consists in two piezoelectric layers. In the real structure, a layer of glue or metal substrate exists between the two piezoelectric ones. However this layer is really thin and can be negligible in front of the other ones. Furthermore, it might be difficult to have precise information on the thickness and mechanical properties of the bonding layer. During the analysis we consider the two piezoelectric layers. In the following, the modelling is separated in two parts: we will firstly consider the modelling of a straight beam under a flexural wave that allows then we consider the complete TWPT and the chaining of transfer matrices to obtain the admittance matrix. In the end, the exploitation methods of this modelling to obtain analytical results are presented.

3.2. Analytical modelling

3.2.1. Straight beam under flexion

The first aspect of the modelling is to consider a straight bimorph beam consisting of two piezoelectric layers as represented in Figure 6. One electrode is located on the superior and one on the inferior faces of the beam. The beam has a length L_k depending on the section considered and a width w. The thickness of each layer is h_p and thus the thickness of the complete beam is $h = 2h_p$. The bimorph under a flexural wave is represented in Figure 7. The wave creates a displacement u_3 in the thickness direction of the beam. During the analysis we consider different mechanical variables that characterize the flexion at the extremities of the beam: the linear velocity U_k, the rotationnal velocity Φ_k, the bending moment M_k and the shear force F_k where K is the electrode ranking. Finally a voltage V_k exists between the two electrodes whether it is applied or generated from the piezoelectric effect and the stress due to the flexural wave. A current I_k also flows through the electrode.

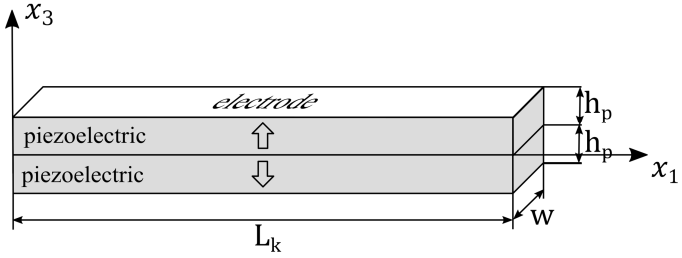

Figure 6. Bimorph beam consisting of two piezoelectric layers

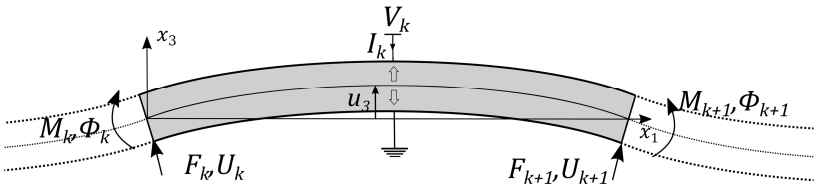

Figure 7. Bimorph beam under flexural wave

The strategy of modeling consists in defining the transfer matrix that links the mechanical variables $(F_{k+1}, M_{k+1}, U_{k+1}, \Phi_{k+1})$ to the ones at the other end of the beam (F_k, M_k, U_k, Φ_k) and the voltage V_k. The Euler-Bernoulli theory and piezoelectric equations are used to achieve this. In order to use this theory several assumptions need to be made :

- we assume that the length L_k is higher than the width and the thickness of the beam

- In order for ring sections to be considered as beams, we assume that the length of each section is small in front of the perimeter of the ring
- Finally we perform an harmonic analysis at pulsation ω.

From the Euler Bernoulli analysis, we can link the bending moment and the shear stress to the displacement u_3 as a function of the position x_1. We have then:

$$M = K_b \frac{\partial^2 u_3}{\partial x_1^2} + N_b V_k \tag{4}$$

$$F = \frac{\partial M}{\partial x_1} = K_b \frac{\partial^3 u_3}{\partial x_1^3} \tag{5}$$

where K_b is the effective bending rigidity of the bimorph and is defined as

$$K_b = \frac{2}{3} \frac{w h_p^3}{s_{p11}^e} \tag{6}$$

with s_{p11}^e the elastic compliance of the piezoelectric material.

N_b characterizes the electromechanical conversion and is defined as:

$$N_b = -\frac{1}{2} w \frac{d_{31}}{s_{p11}^e} h_p \tag{7}$$

with d_{31} the piezoelectric coefficient as we only consider the transverse vibration mode.

The definition of the moment and shear stress then leads us to the propagation equation for u_3:

$$K_b \frac{\partial^4 u_3}{\partial x_1^4} + \rho_p w h \frac{\partial^2 u_3}{\partial t^2} = 0 \tag{8}$$

with ρ_p the density of the piezoelectric material.

The resolution of the equation gives the displacement u_3 as a function of the position along the bimorph x_1:

$$u_3 = \left[\alpha_1 \cos\left(\frac{2\pi x_1}{\lambda}\right) + \alpha_2 \sin\left(\frac{2\pi x_1}{\lambda}\right) + \alpha_3 \cosh\left(\frac{2\pi x_1}{\lambda}\right) + \alpha_4 \sinh\left(\frac{2\pi x_1}{\lambda}\right)\right] e^{j\omega t} \tag{9}$$

λ is the wavelength of the wave and is equal to:

$$\lambda = 2\pi \left(\frac{K_b}{\rho_p w h \omega^2}\right)^{\frac{1}{4}} \tag{10}$$

λ is depending on the mechanical and geometric properties of the ring and will be the same for all the sections and thus for the complete piezoelectric transformer.

The coefficients α_i depend on the limit conditions at each side of the beam section, i.e. the mechanical variables $(F_k,\ M_k\ , U_k, \Phi_k)$. The first step consists in determining these α_i. We can obtain a system of four equations by considering the angular and linear velocities at each side of the beam. Indeed we have:

$$\begin{aligned} U_k &= \left.\frac{\partial u_3}{\partial t}\right|_{x_1=0}, \qquad U_{k+1} = \left.\frac{\partial u_3}{\partial t}\right|_{x_1=L_k} \\ \Phi_k &= -\left.\frac{\partial u_3}{\partial t \partial x_1}\right|_{x_1=0}, \qquad \Phi_{k+1} = -\left.\frac{\partial u_3}{\partial t \partial x_1}\right|_{x_1=L_k} \end{aligned} \tag{11}$$

Thus, by replacing u_3 with **(9)** and solving the system we can directly link the α_i to $(U_k, \Phi_k, U_{k+1}, \Phi_{k+1})$:

$$\begin{pmatrix}\alpha_1\\ \alpha_2\\ \alpha_3\\ \alpha_4\end{pmatrix} = A_k \begin{pmatrix} U_k\\ \Phi_k\\ U_{k+1}\\ \Phi_{k+1}\end{pmatrix} \tag{12}$$

Now the displacement u_3 is completely defined by the velocities at the boundaries. Then by using **(4)** and **(5)**, we express the shear stresses and flexural moments at boundaries as a function of the α_i and thus as a function of the velocities. In the end we obtain a matrix linking the moments and stresses to the velocities and to the voltage V_k. By reorganizing the system of equations we can obtain a system defined by the following equation:

$$\begin{pmatrix}F_k\\ M_k\\ U_k\\ \Phi_k\end{pmatrix} = G_{L_k} \begin{pmatrix} F_{k+1}\\ M_{k+1}\\ U_{k+1}\\ \Phi_{k+1}\end{pmatrix} + P_{L_k} V \tag{13}$$

where the mechanical variables at one side are expressed as a function of the mechanical variables at the other side and the voltage V_k. The matrices G_{L_k} and P_{L_k} are defined as follow:

$$G_{L_k} = \frac{1}{2}\begin{pmatrix} m+c & -\lambda(n-s) & \frac{K_b\lambda^3(n+s)}{j\omega} & \frac{K_b\lambda^2(m-c)}{j\omega}\\ -\frac{(n+s)}{\lambda} & m+c & -\frac{K_b\lambda^2(m-c)}{j\omega} & \frac{-K_b\lambda(n-s)}{j\omega}\\ \frac{j\omega(n-s)}{K_b\lambda^3} & \frac{-j\omega(m-c)}{K_b\lambda^2} & m+c & \frac{(n+s)}{\lambda}\\ \frac{j\omega(m-c)}{K_b\lambda^2} & \frac{-j\omega(n+s)}{K_b\lambda} & \lambda(n-s) & m+c\end{pmatrix} \tag{14}$$

$$P_{L_k} = \frac{N_b}{2}\begin{pmatrix} \frac{\lambda(n-s)}{2}\\ 2-(m+c)\\ \frac{j\omega(m-c)}{K_b\lambda^2}\\ \frac{j\omega(n+s)}{K_b\lambda}\end{pmatrix} \tag{15}$$

with $c = \cos\left(\frac{2\pi L_k}{\lambda}\right)$ $s = \sin\left(\frac{2\pi L_k}{\lambda}\right)$ $m = \cosh\left(\frac{2\pi L_k}{\lambda}\right)$ $n = \sinh\left(\frac{2\pi L_k}{\lambda}\right)$.

We can note some relations between those chain matrices:

$$\begin{aligned} G_{L_k}.G_{L_{k+1}} &= G_{L_k+L_{k+1}}\\ G_{L_k}.P_{L_{k+1}} &= P_{L_k+L_{k+1}} - P_{L_k}\end{aligned} \tag{16}$$

3.2.2. Admittance matrix for a closed chain of beam sections

Each section of a ring can be defined now by the couple (V_k, I_k) and the transfer matrix that depends on the length of the ring. The length of the ring is linked to its circumference which is different if we consider the interior or exterior radius. We must determine an equivalent diameter to determine the length in the modelling. This equivalent diameter parameter is chosen between the internal diameter and external diameter in order to obtain the same theoretical resonant frequency for the modelling presented than the natural resonant frequency of the ring. The natural resonant frequency of the ring can be found analytically [28] or by FEM. The equivalent diameter D_e is then linked to the wavelength λ and is obtained as follows:

$$\lambda = \frac{Perim}{3} = \frac{D_e \pi}{3}$$
$$D_e = 6\left(\frac{K_b}{\rho_p w h \omega^2}\right)^{\frac{1}{4}} \tag{17}$$

For straight transformers as in [27], the admittance matrix is obtained by chaining the matrices. At the extremities of the transformer, fixed boundary conditions apply and the resolution of the system of equation results in the definition of the admittance matrix Y_{tot}. In the present case, no boundary conditions applied as the propagation medium is continuous. However, the resolution method based on the chaining of transfer matrices relevant, only the system of equations will be different.

This method of resolution is generic and applies to a ring-type piezoelectric transformer with any number of electrodes with variable length as long as the assumptions made before remain valid. In the general case we will consider a piezoelectric ring consisting of n electrodes. To simplify the notations we consider the matrix B_k that represents the mechanical variables at the interface between electrodes k and k+1:

$$B_k = \begin{pmatrix} F_k \\ M_k \\ U_k \\ \Phi_k \end{pmatrix} \tag{18}$$

The scheme of matrix chaining we use is represented in Figure 8.

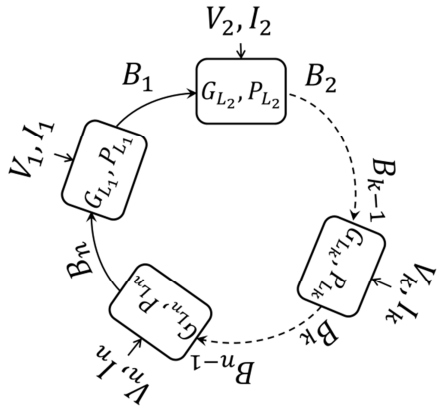

Figure 8. Matrix chaining scheme of the TWPT with n electrodes

Using this scheme, we can start by expressing B_1 as:

$$B_1 = G_{L_1} B_n + P_{L_1} V_1 \tag{19}$$

Then we obtain B_2:

$$\begin{aligned} B_2 &= G_{L_2} B_1 + P_{L_2} V_2 = G_{L_2} G_{L_1} B_n + P_{L_2} V_2 + G_{L_2} P_{L_1} V_1 \\ &= G_{L_2+L_1} B_n + \left(P_{L_2+L_1} - P_{L_2}\right) V_1 + P_{L_2} V_2 \\ &= G_{L_2+L_1} B_n + TT_2 V \end{aligned} \tag{20}$$

with the help of the formulas **(16)**. We introduce the matrix TT_k which is a 4×n matrix that links the matrix B_k to the vector V that contains all the voltages. For the second electrode we have then:

$$TT_2 = \begin{pmatrix} \left(P_{L_2+L_1} - P_{L_2}\right) & P_{L_2} & 0 & \cdots & 0 \end{pmatrix} \tag{21}$$

$$V = \begin{pmatrix} V_1 \\ \vdots \\ V_k \\ \vdots \\ V_n \end{pmatrix} \tag{22}$$

The following B_k can be expressed in the same way as a function of B_n and all the voltages V_i. The final equation we obtain is then:

$$B_n = G_{L_{tot}} B_n + TT_n V \tag{23}$$

with $L_{tot} = L_n + \cdots + L_k + \cdots + L_1$ corresponding to the perimeter of the ring, TT_n a 4×n matrix. The matrix TT_n is expressed as:

$$\begin{aligned} &TT_n \\ &= \begin{pmatrix} \left(P_{L_n+\cdots+L_1} - P_{L_n+\cdots+L_2}\right) & \left(P_{L_n+\cdots+L_2} - P_{L_n+\cdots+L_3}\right) & \cdots & \left(P_{L_n+\cdots+L_k} - P_{L_n+\cdots+L_{k+1}}\right) & \cdots & P_{L_n} \end{pmatrix} \end{aligned} \tag{24}$$

Thus, at the end of the chaining we obtain a relation expressing B_n as a function of B_n and V. We can solve for B_n and obtain:

$$B_n = \left(I_d^n - G_{L_{tot}}\right)^{-1} TT_n V = P_{fn} V \tag{25}$$

All the matrices B_k are expressed as a function of B_n in the process explained previously thus all the mechanical variables $(F_k,\ M_k\ , U_k, \Phi_k)$ around the circumference of the piezoelectric transformer can be determined as a function of V.

$$B_k = G_{L_k+\cdots+L_1} P_{fn} V + TT_k\ V = \left(G_{L_j+\cdots+L_1} P_{fn} + TT_k\right) V = P_{fk} V \tag{26}$$

To obtain the admittance matrix, the currents must be determined as a function of the voltages. From the piezoelectric equations, we have the following formula for the current flowing through an electrode as a function of the voltage V_k and the rotational velocities at both sides of the section.

$$I_k = j\omega C_k V_k + N_b(\Phi_{k+1} - \Phi_k) \tag{27}$$

where C_k is the equivalent capacitance of the considered ring section and is equal to:

$$C_k = \varepsilon_{33}\left(1 - \frac{d_{31}^2}{s_{p11}^e \varepsilon_{33}}\right)\frac{wL_k}{2h_p} \tag{28}$$

and ε_{33} the dielectric permittivity of the piezoelectric material.
The combination of equations (26) and (27) results in the determination of the complete admittance matrix Y_{tot} whose parameters depend on the geometrical and material properties of the structure and is not detailed here.

$$I = Y_{tot} V \tag{29}$$

3.3. Admittance matrix applied to the piezoelectric transformer

The admittance matrix determines completely the coupling between electrodes and the electrical behavior of the transformer. It does not take into account whether electrodes are inputs or outputs. In practical, Y_{tot} does not have a formal expression and its determination is made numerically following the process detailed before. From this admittance matrix, we can extract numerically the electrical quantities and performances of the transformer. Firstly, electrodes must be set as inputs or outputs. For input electrodes, we used phasor representation of the voltage. For output electrodes, we can only consider any linear loads (RLC circuits) to perform numeric resolution. In the following we will

consider only a resistive load. The aim of the numeric resolution is to determine the missing electrical quantities: the voltages across output electrodes and the currents through input electrodes that allow then complete determination of the electrical behavior of the transformer.

If we consider a TWPT with only one output electrode k with a resistive load, the current flowing is linked to the voltage by **(30)** corresponding to the representation of Figure 5.

$$I_k = -\frac{V_k}{R_k} \tag{30}$$

Thus, the relation **(29)** becomes

$$\begin{pmatrix} I_1 \\ \vdots \\ -\frac{V_k}{R_k} \\ \vdots \\ I_n \end{pmatrix} = Y_{tot} \begin{pmatrix} V_1 \\ \vdots \\ V_k \\ \vdots \\ V_n \end{pmatrix} \tag{31}$$

and we have for V_k:

$$\begin{aligned} -\frac{V_k}{R_k} = Y_{tot,k} \begin{pmatrix} V_1 \\ \vdots \\ V_k \\ \vdots \\ V_n \end{pmatrix} = Y_{tot,(k,k)} V_k + Y_{tot,(k,(1:n)-\{k\})} \begin{pmatrix} V_1 \\ \vdots \\ \vdots \\ V_n \end{pmatrix} \\ V_k = -\left(\frac{1}{R_k} + Y_{tot(k,k)}\right) Y_{tot,(k,(1:n)-\{k\})} \begin{pmatrix} V_1 \\ \vdots \\ \vdots \\ V_n \end{pmatrix} \end{aligned} \tag{32}$$

If all other electrodes are inputs then we can solve for V_k and find its complex amplitude. If the number of output electrodes is higher, the process remains the same to determine the complex amplitude of the output voltages. This resolution allows determining numerically the output voltages and then the complex amplitude of the input and output currents can be determined with **(29)**. As we are working with complex amplitude we can numerically determine directly the input and output power to characterize completely the performances of the piezoelectric transformer.

3.4. Mechanical behaviour extraction

The modelling presented here not only allows for evaluation of the electrical behaviour of the transformer but also its mechanical one. Especially, the important mechanical quantities in the design of the piezoelectric transformer are the vertical displacement $u_3$and moreover the stress T_1in the piezoelectric material. As stated before, when the input voltages and output loads are defined, we can determined all the voltages on the electrodes **(32)** and furthermore, all the mechanical variables Bk along the circumference of the ring **(26)** and thus the α_i for each ring section **(12)**. With the α_i determined, we can thus obtain the displacement u_3 of each point on the transformer with equation **(9)**.

The stress T_1 in the piezoelectric transformer is determined with the help of piezoelectric equations we have indeed :

$$T_1 = \frac{S_1}{s^e_{p11}} - \frac{d_{31}}{s^e_{p11}} E_3 \tag{33}$$

With $S_1 = -z\frac{\partial^2 u_3}{\partial x_1^2}$ the deformation, E_3 the electric field and z the position considered in the thickness direction. When replacing, we obtain the stress in the ring section k as a function of the displacement and the voltage applied:

$$T_{1,k}(z,x_1) = -\frac{1}{s^e_{p11}}\left(z\frac{\partial^2 u_{3,k}(x_1)}{\partial x_1^2} + \frac{d_{31}V_k}{2h_p}\right) \tag{34}$$

4. Experimental Validation

4.1. Setup Description

In order to validate the concept and the analytical modelling, a piezoelectric transformer is made and tested. The tests are performed with output resistive load and input sinusoidal voltages to compare the results obtained experimentally and by analytical modelling and validate the operation of the transformer in traveling wave. No further depth was put on its sizing to optimize the electrical performances. The piezoelectric transformer designed is shown in Figure 9 with its interface circuit. It consists in two piezoelectric rings with twelve silver electrodes on its upper and lower surfaces.

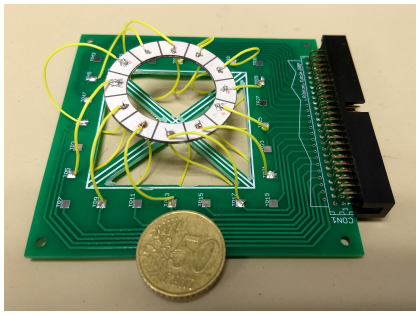

Figure 9. Traveling Wave piezoelectric transformer with its interface PCB board

The material properties and sizes are presented in Table 1 and Table 2. In order to facilitate the creation of a flexural wave, the piezoelectric layers are chosen as thin as possible with a thickness $h_p = 500$ µm. The width of the piezoelectric ring is $w = 6.5$ mm and the external diameter is 40 mm.

The two layers are bonded together with a silver epoxy conductive adhesive that ensures the mechanical coupling between the two layers and the continuity of the electric field in the piezoelectric material. The bonding of the wires on the electrodes is conducted with a Sn/Ag/Cu solder that melts at 240°C, that is to say much below the Curie point of the piezoelectric material ($T_c = 320$°C) and allows for good bonding on the silver electrodes. The piezoelectric transformer is then connected to an interface PCB with a connector to carry reproducible tests. The complete transformer thus is maintained in position by the wire tension and we consider thus that no stress is put on the inferior and superior surface.

Table 1: Properties of the piezoelectric material (from datasheet)

Parameter	Value	Units	Notation
Density	7500	kg/m^3	ρ_p
Elastic Compliance	0.119×10^{-12}	m^2/N	s^e_{p11}
Permittivity	$1135\varepsilon_0$	F/m	ε_{33}
Dielectric constant	-0.139×10^{-9}	C/N	d_{31}

Table 2: Geometric parameters of the TWPT

Parameter	Value	Units	Notation
Width	6.5	mm	w
Thickness of one piezoelectric layer	0.5	mm	h_p
Inner Radius	13.5	mm	R_i
Outer Radius	20	mm	R_o

With this number of electrodes, our aim is to excite the third mode of resonance of the transformer as shown in Figure 4. The geometry of the electrodes and the inputs and outputs scheme is presented in Figure 10 and is identical to the one presented in Figure 2 a). There are small differences with the generic case presented before. In order to generate the traveling wave, we need four voltages. The need for opposite voltages is explained by the electrode geometry compared to the resonance mode waveform. When electrode 1 corresponds to a high antinode of the resonance mode, electrode 3 corresponds to a low antinode. Thus, in order to drive the standing wave we need opposite voltages. In practical, it will be possible to polarize the piezoelectric transformer in opposite directions directly during the fabrication process to only need two supply voltages.

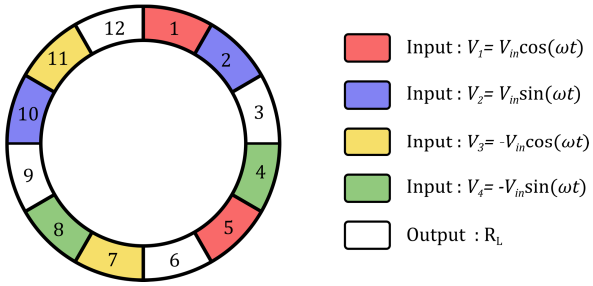

Figure 10. Electrode scheme on the experimental TWPT

The complete circuit of test is presented in Figure 11. The generation of the signals is made by an arbitrary function generator. It generates the two signals V_{g1} and V_{g2} with a 90° phase shift. Two inverters allow to obtain the four signals that are input into linear power amplifiers to generate the sinusoidal voltages that will supply the piezoelectric transformer. As contrary to the modelling where we considered the inferior electrode connected to the ground, here the inferior electrode is connected to the opposite of the voltage on the superior electrode. The aim is to double the electric field in the piezoelectric material. We will only now consider the amplitude V_{in} as the double of each driving signal. The secondary electrodes of the transformer are loaded with resistances. The measurements are performed over a frequency range between 3.5 and 4.5 kHz around the resonance of the structure with varying resistive loads and input voltages. With this set up we measure the output voltages as well as the input currents and voltages and the phase shift between them to obtain power and efficiency results.

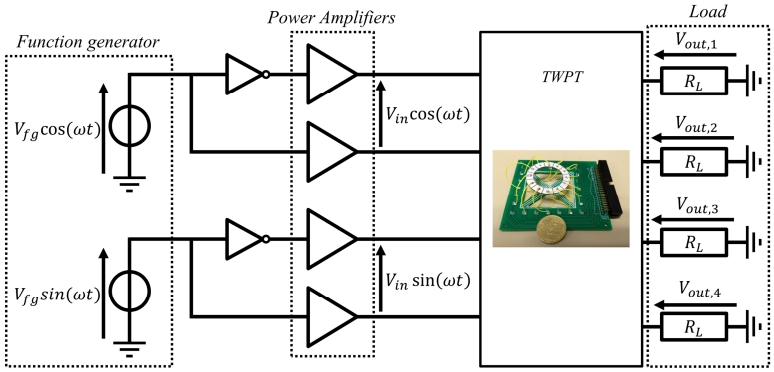

Figure 11. Electrical circuit of testbench for the TWPT

4.2. Losses consideration

The losses are a key aspect as this transformer will be used in power converter application. They are present in the form of piezoelectric, mechanic and dielectric losses. They are mainly dependent on the material properties. In the mechanical analysis and in the datasheet of the piezoelectric material, losses are taken into account in the form of complex representation of the material properties. The piezoelectric losses are in general negligible in front of the two other ones and not consider in the analysis. Thus we introduce the elastic loss coefficient δ_m and the dielectric loss one δ_e such that we have for the piezoelectric material elastic compliance and permittivity:

$$\begin{aligned} \tilde{s}^e_{p11} &= (1 - j\delta_{m,p}) s^e_{p11} \\ \tilde{\varepsilon}_{33} &= (1 - j\delta_{e,p}) \varepsilon_{33} \end{aligned} \tag{35}$$

These coefficients are given by the piezoelectric element manufacturer. However, in the piezoelectric transformer considered here, other parameters have an impact on the losses. The bonding of the two piezoelectric rings induces new losses due to the material properties of the adhesive and to the quality of the bonding. We can also add that the bonding of the wire with the solder also adds losses to the complete losses of the transformer. In the end, the coefficients given by the manufacturer for the loss coefficient in the piezoelectric material aren't close to the practical one. Note that the bonding of the two piezoelectric layers and of the wire was conducted in our lab and with industrial process, less parasitic losses would appear.

In order to feed the values to our modeling of the transformer, we extract the loss coefficients directly from measurements on the transformer to test the validity of the model with the same loss coefficients. The method used is based on admittance measurements of the piezoelectric transformer [29]. What we expect is to have a close evaluation of those coefficients without putting too much emphasis on strong precision. The dielectric loss parameter is found outside the resonance from the measurement of the series parasitic capacitance and the capacitance of the piezoelectric transformer. This coefficient is normally dependent on the frequency but we consider here that it remains constant in the frequency range studied. The mechanical loss factor is found at resonance and depends on the minimum and maximum absolute admittance values, respectively $|Y_{min}|$ and $|Y_{max}|$ and the pulsations at which they appear, f_{min} and f_{max} as represented in Figure 12. The graph has been obtained by measuring the impedance of the complete transformer with an impedance analyzer. The loss coefficients are summarized in Table 3.

$$\delta_{m,p} = \frac{2(f_{min} - f_{max})}{f_{max}} \sqrt{\frac{|Y_{max}|}{|Y_{min}|}} \tag{36}$$

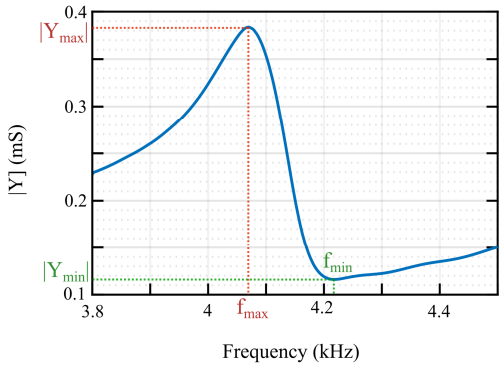

Figure 12. Admittance of the piezoelectric transformer for losses determination

Table 3: Losses Parameters of the TWPT

Parameter	Value	Units	Notation
Dielectric loss coefficient	0.005	Ø	$\delta_{e,p}$
Mechanical loss coefficient	0.04	Ø	$\delta_{m,p}$

4.3. Measurement results and comparison with modelling results

4.3.1. Transient Analysis

The first aspect of the experimental set-up was to validate the concept of the traveling wave piezoelectric transformer. Thus, in Figure 13 is represented the output voltages as a function of time for an input amplitude of 20 V, a load resistance of 56 kΩ and at a frequency of 4.1 kHz. We note on this graph, that we have four voltages with a $\frac{\pi}{2}$ phase shift between them thus validating the behaviour with a traveling wave. However, there are several differences in terms of amplitude between the phases. These differences can be greater than represented on the Figure 13 depending on the frequency and come from differences in the fabrication process of the transformer. The bonding might not be homogenous along the circumference of the ring. Furthermore, the bonding of wire on the electrodes surface is different between electrodes. This leads to difference in quality factor for each ring section and overall for each system of electrodes. We will see after that this also affects the frequency response of the transformer as the mass of the silver bonding also plays a role on the resonance of each system.

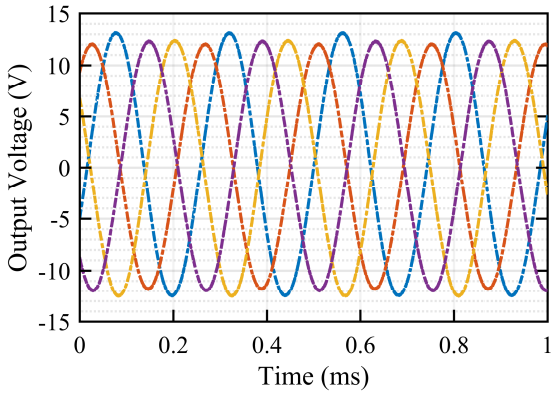

Figure 13. Observed waveforms of the output voltage of the transformer

4.3.2. Harmonic and multimodal analysis

The second aspect of the experimentation was to confront measurements to results obtained with the analytical modelling. We considered several aspects in this comparison. The first one was a good anticipation of the resonances of the transformer and of the traveling wave behaviour. The second one was a good correlation in the evolution of the electric quantities when varying parameters such as the load resistance or the input voltage. The results of the analytical modelling are obtained with the geometric parameters and material properties presented in Table 1 and 2. The same input voltage scheme is used with complex amplitudes representing the different phases at the input. The first comparison is shown in Figure 14. In this graph, we represented the amplitude of the output voltages over a broader range of frequencies as measured and obtained by the modelling. For the rest of the article, when talking about output voltages, we consider the amplitude of the signals. For the modelling we only get one curve as the there is no differences in terms of gain between the outputs only a difference in phase. The first resonant frequency is well anticipated with slight differences in term of absolute value. It corresponds to the 3rd mode of resonance as represented in Figure 4. That's the one we will consider in the following as it presents the best electrical performances in terms of power transfer. The second resonance observe in the experiment corresponds to the 4th mode. It is not present in the modelling due to perfect assumed symmetries in the electrodes and to the pattern chosen. The standing waves cancelled each other and mathematically we do not observe the 4th mode. In the experiment, even though the symmetry is the same, the irregularities make it so that we observe this resonance. Finally the last resonance is the 5th mode and is predicted by the model with differences in terms of resonant frequency due to the assumptions made, i.e. we considered ring sections as straight beams. With the zoom of the 3rd mode resonance, we see firstly that the absolute value of the voltage given by the modelling is higher than the ones measured. This is directly related to the evaluation of losses and especially characterization of the bonding between the layers. Furthermore, we see a difference in terms of resonance for the phases that are separated in two groups. This is related to the independent standing waves discussed in section 2. There are two independent systems and the output phases directly relate to one or another and for the different systems, the mechanical properties can be different, e.g. the bonding of the wires can add weight on the surface and shift the resonant frequency.

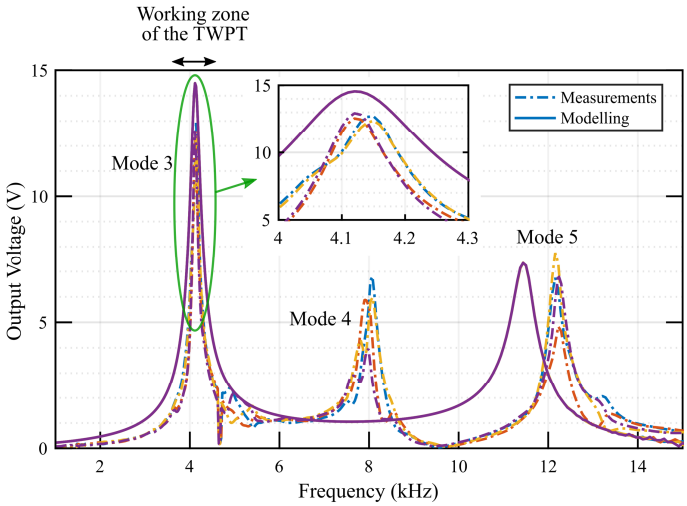

Figure 14. Output voltage as a function of the frequency for experimental and analytical modeling

4.3.3. Influence of the input voltage V_{in} and load resistance R_L

To continue the experimental validation of the TWPT, we limit now to the frequency range around the resonance for the 3rd mode where the TWPT will be used in the targeted aoolication and see the influence of the different parameters. In Figure 15, we focus on the influence of the load resistance on the output voltage of the transformer for an input voltage of 20 V. We compare the measurements for one output voltage and the modelling results. Considering the absolute value of the output voltages, we note that the model fit quite well but there are still differences in terms of maximum voltage and resonance behavior, notably the quality factor. Moreover, the evolution of the voltage as a function of the resistance follows the same pattern for the two results. When the resistance increases, the output voltage increases and the resonant frequency gets higher. The second aspect is observable notably for $R_L = 470\ \text{k}\Omega$. In general the modelling results and measurements fit quite well in the range of resistance studied. We focus then on the evolution of the output voltage depending on the input voltage in Figure 16 for a load resistance of 56 kΩ. When the input voltage increases, the output voltage also increases as expected. We can comment on the shape of the output voltage measured as a function of the frequency. For low voltages, we see that there isn't a clear peak but an evolution in two times. This shape comes from the phase-shift in resonance of the two electrodes system considered before. Their peak resonances do not appear at the same frequency which leads to the evolution observed here.

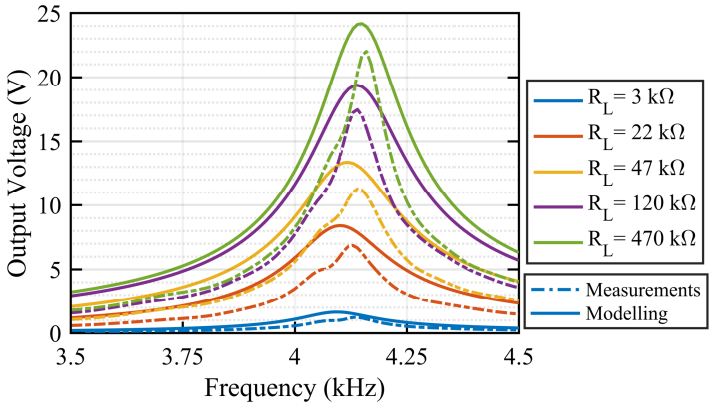

Figure 15. Evolution of the output voltage as a function of the load resistance for the experimentation and analytical modeling for $\boldsymbol{V_{in} = 20\ V}$

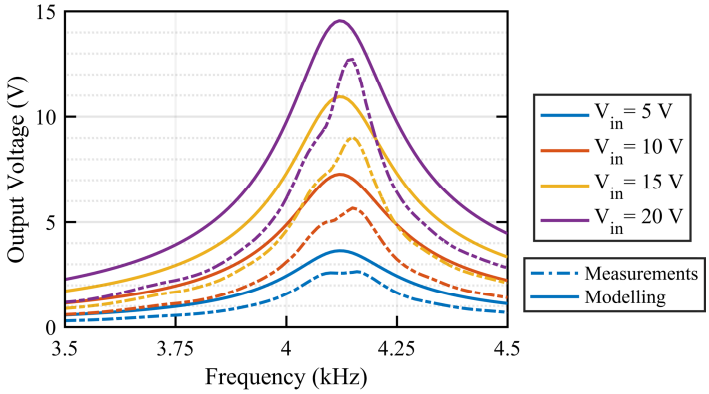

Figure 16. Evolution of the output voltage as a function of the input voltage for the experimentation and analytical modeling for $\boldsymbol{R_L = 56\ k\Omega}$

4.3.4. Maximum power point

As we compared the modelling and experimental results for the output voltages, we will now compare the power performances of the transformer. In Figure 17, is represented the evolution of maximum power and maximum voltages as a function of the load resistance as predicted by the modelling and measured experimentally. As for the results presented before, there is a difference in terms of absolute values between the two, however, the maximum power point is obtained for the same optimum load resistance value. The maximum power that we obtain with our TWPT is of 5.5 mW and the maximum efficiency in this case is of 15%.

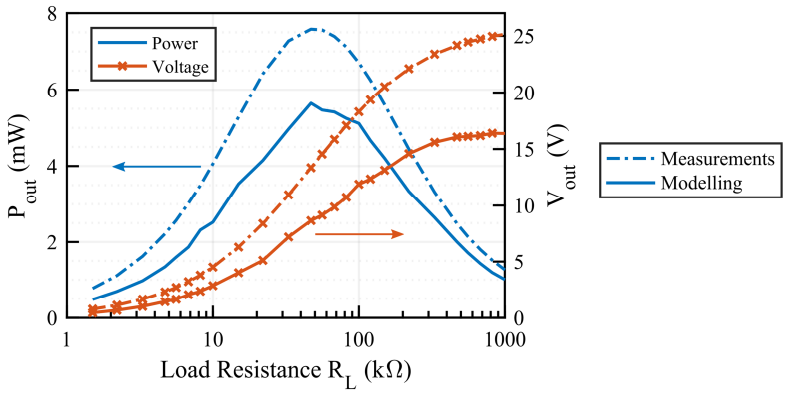

Figure 17. Evolution of the output voltage and power as a function of the load resistance $\boldsymbol{R_L}$

4.3.5. Mechanical performances

We can link the optimum power to the displacement and stress in the piezoelectric material. We computed the maximum displacement and stress in the piezoelectric transformer from the modelling analysis (33) and from finite element analysis as a function of the load resistance in Figure 18. The FEM model presents the same geometric properties and the material properties are the one given by the manufacturer. The two mechanical quantities follow the same behaviour for the analysis with a value of the load resistance that gives the minimum of both. This value of the load resistance corresponds to the maximum output power as evaluated in Figure 17. When the electrical power is maximum, less energy is present in the mechanical domain and the amplitudes of the displacement and stress decrease. There exist several differences in terms of absolute value between the FEM and the modelling due to the 3D nature of the FEM method compared to the modelling and furthermore due the losses taken into account. In the FEM model, we only consider losses coefficient for the compliances $s_{11}$and s_{22} leaving the other parameters lossless. The mechanical quantities were not measured on the system for comparison.

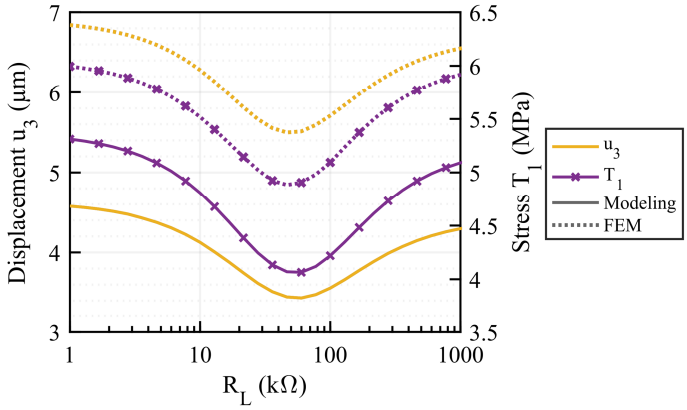

Figure 18. Displacement and stress in the piezoelectric transformer as a function of the load for the modelling and FEM

5. Analytical model to support TWPT design optimization

The experimental results presented in the previous section validate the analytical modelling. This allows now the use of the modelling for the design and optimization of the piezoelectric transformer. Firstly it rises the question of the performances attainable by the TWPT. As stated before, the studied transformer was realized in our lab and presents many losses especially mechanically. One key aspect remains the anticipation of the losses in the TWPT notably considering the bonding of the piezoelectric layers but with industrial process, it is safe to expect very lower mechanical losses coefficients that would lead to better efficiency and thus more transmitted power. In Figure 19 we represent the maximum output power attainable as a function of the loss coefficient given by the modelling. With the loss coefficient we measured, the maximum power attainable was of a few mW. If we take the loss coefficient given by the datasheet $\delta_{m,p,th} = 0.63 \times 10^{-3}$ for the ceramic, the output power would be 650 mW. Obviously, the loss coefficient is for the ceramic alone and does not take into account all the bonding process but it constitutes a maximum theoretical power attainable by the transformer. This also shows the important influence of the mechanical quality factor and thus the mechanical loss coefficient of the material on the performances of the transformer.

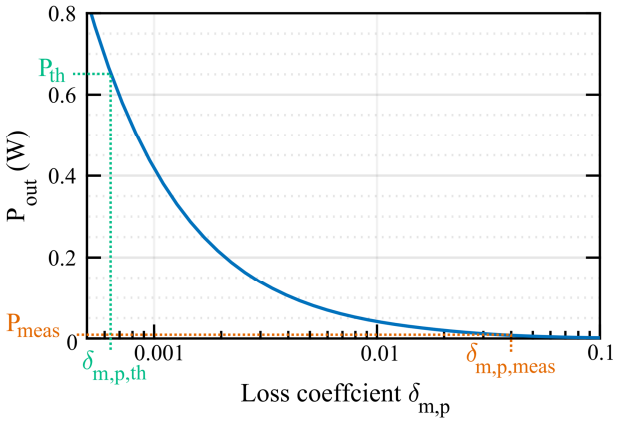

Figure 19. Maximum output power as function of the mechanical loss coefficient from the modelling

Furthermore, one key aspect in the design of piezoelectric transformer is the power density. With our modelling, we explore the influence of the form factor of the piezoelectric transformer. It meas that starting from the geometric parameters presented in **Table 2**, when we choose a thickness h_p of 0.25 mm instead of 0.5 mm all the other parameters are divided by two. The shape of the piezoelectric transformers does not change only its size. The parameter for the reduciton of the size of the transformer is the thickness h_p and we represent on Figure 20 a), the maximum power obtainable by the piezoelectric transformer as a function of this size reduction parameter. We notice that from the modelling the power remains the same and thus the power density increases drastically when reducing the size of the transformer. The maximum power obtainable depends only on the ratio between the output and internal radius. On Figure 20 b) is also represented the stress in the piezoelectric transformer that increases as the size of the transformer decreases. Thus, even though the volume of the transformer decreases, the stress and the working frequency increases that leads to a constant output power irrespective of the size. However, those results only take account of the electro-mechanical aspect of the transformer and the thermal conditions. In practical, the power density of a transformer is limited by thermal conditions. In Figure 20 b) the thermal flux is also represented as a function of the form factor and as expected, when the size of the trasnformer decreases, the thermal flux increases and will limit the reduction of the size of the transformer.

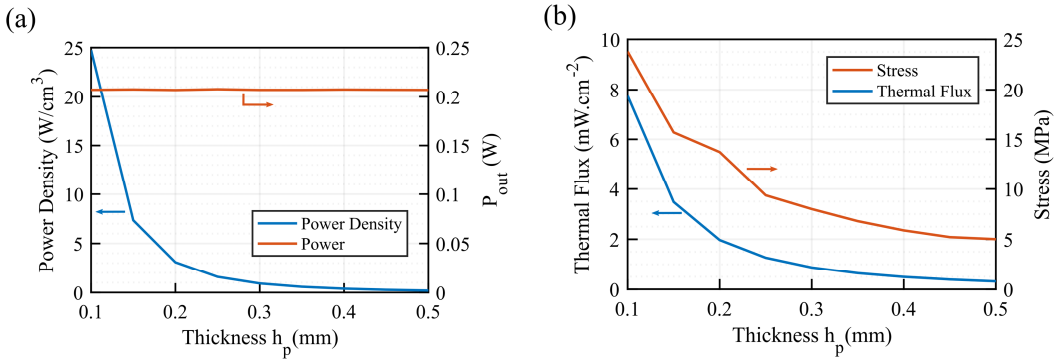

Figure 20. (a) Power and power density and (b) Thermal flux and maximum stress in the piezoelectric transformer as a function of the form factor

Finally, the experimental electrode scheme only allows for four phases at the output when it's theoretically possible to obtain as much as wanted. In Figure 21, we represented the output voltages we could obtain with an electrode scheme similar to the one presented in Figure 3 c) and with a mechanical loss coefficient $\delta_{m,p} = 0.001$. We can see here clearly that we could obtain 8 output voltages. No limitations is put on the number of phases obtainable at the output, but the output voltage and power available for each electrodes decrease as the number of phases increase.

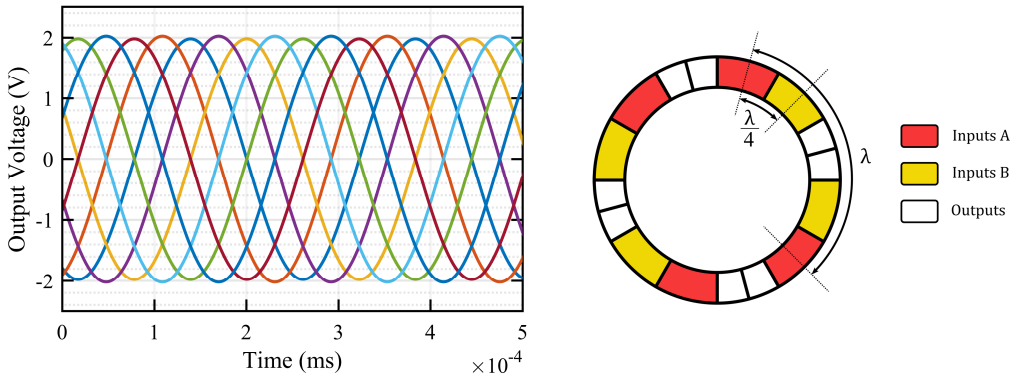

Figure 21. Theoretical octophase system obtainable with the TWPT with the proposed electrode scheme for $\boldsymbol{V_{in} = 20\ V}$ and $\boldsymbol{R_L = 7.5\ k\Omega}$

6. Conclusion

A new concept of piezoelectric transformer is proposed in this paper which performs the electromechanical coupling through the use of a flexural traveling wave as contrary to a standing wave for classic topologies. It consists in two piezoelectric rings polarized in opposite direction and bonded together. This propagation mode allows obtaining a multi-phase system at the output thus opening the possibility of a universal power converter able to realize different kind of conversions: polyphase rectification, DC-AC conversion with variable frequency at the output. Due to the novelty of the architecture, an analytical modelling of the transformer is proposed which characterizes its behaviour through an admittance matrix close to the representation of two-port network. This modelling allows foreseeing the performance of the TWPT with numerical frequency-domain analysis. Furthermore, with the representation with an admittance matrix, it would be also possible to perform time-domain simulations and use it in a simulation of the complete power converter.

The concept of the TWPT and its modelling were validated experimentally. The proposed TWPT outputs a 4 phases system of voltages with an optimum power of 5.5 mW for a thickness of 1mm and a 40mm diameter. The evolutions of the performances as a function of the load or the input voltage follow the same pattern in the modelling and experiment and the optimum power is reached for the same optimum load in the two cases. The TWPT was not designed for optimization of the electrical performances but only for validation and present many losses due to the fabrication process of the transformer. However, the maximum theoretical performances attainable are much higher and it can reach very high power density. The theoretical power obtainable for the same dimensions and material is 650 mW. With industrial process of fabrication and good choice of sizes and material properties, better performances can be expected with versatility in the electrodes scheme to obtain any number of phases at the output.

7. References

[1] Wells E. 2002 Comparing magnetic and piezoelectric transformer approaches in CCFL applications *Texas Instruments Analog Appl. J.*

[2] Flynn A M and Sanders S R 2002 Fundamental limits on energy transfer and circuit considerations for piezoelectric transformers *IEEE Trans. Power Electron.* **17** 8–14

[3] Vasic D, Costa F and Sarraute E 2006 Piezoelectric transformer for integrated MOSFET and IGBT gate driver *IEEE Trans. Power Electron.* **21** 56–65

[4] Su Y-H, Liu Y-P, Vasic D, Costa F, Wu W-J and Lee C-K 2013 Study of a piezoelectric transformer-based DC/DC converter with a cooling system and current-doubler rectifier *Smart Mater. Struct.* **22** 95005

[5] Alonso J M, Ordiz C, Dalla Costa M A, Ribas J and Cardesin J 2007 High Voltage Power Supply for Ozone Generation Based on Piezoelectric Transformer *2007 IEEE Industry Applications Annual Meeting* (IEEE) pp 1901–8

[6] Itoh H, Teranishi K and Suzuki S 2006 Discharge plasmas generated by piezoelectric transformers and their applications *Plasma Sources Sci. Technol.* **15** S51–61

[7] Martinez T, Pillonnet G and Costa F 2018 A 15-mV Inductor-Less Start-up Converter Using a Piezoelectric Transformer for Energy Harvesting Applications *IEEE Trans. Power Electron.* **33** 2241–53

[8] Camarda A, Tartagni M and Romani A 2018 A −8 mV/+15 mV Double Polarity Piezoelectric Transformer-Based Step-Up Oscillator for Energy Harvesting Applications *IEEE Trans. Circuits Syst. I Regul. Pap.* **65** 1454–67

[9] Bedair S S, Pulskamp J S, Polcawich R G, Rudy R Q and Puder J 2015 Thin-film piezoelectric transformers operating in harmonics of out-of-plane flexure modes *2015 Transducers - 2015 18th International Conference on Solid-State Sensors, Actuators and Microsystems (TRANSDUCERS)* (IEEE) pp 714–7

[10] Camarda A, Sordo G, Iannacci J, Schneider M, Schmid U, Tartagni M and Romani A 2017 Fabrication and Electromechanical Modeling of a Flexural-Mode MEMS Piezoelectric Transformer in AlN *J. Microelectromechanical Syst.* **26** 1110–21

[11] Kauczor C, Schulte T and Grotstollen H 2003 Piezoelectric Transformer of Travelling Wave Type *Actuator 2004* pp 395–8

[12] Hagedorn P and Wallaschek J 1992 Travelling wave ultrasonic motors, Part I: Working principle and mathematical modelling of the stator *J. Sound Vib.* **155** 31–46

[13] Ro J-S, Yi K-P, Chung T-K, Jung H-K and Jung H-K 2013 Characteristic analysis and shape optimal design of a ring-type traveling wave ultrasonic motor *Eur. Phys. J. Appl. Phys.* **63** 10901

[14] Peng T, Shi H, Liang X, Luo F and Wu X 2015 Experimental investigation on sandwich structure ring-type ultrasonic motor *Ultrasonics* **56** 303–7

[15] Duan W H, Quek S T and Wang Q 2009 A novel ring type ultrasonic motor with multiple wavenumbers: design, fabrication and characterization *Smart Mater. Struct* **18** 125025–13

[16] Smith G L, Rudy R Q, Polcawich R G and DeVoe D L 2012 Integrated thin-film piezoelectric

traveling wave ultrasonic motors *Sensors Actuators A Phys.* **188** 305–11
[17] Wang L, Wielert T, Twiefel J, Jin J and Wallaschek J 2017 A rod type linear ultrasonic motor utilizing longitudinal traveling waves: proof of concept *Smart Mater. Struct.* **26** 85013
[18] Park S and He S 2012 Standing wave brass-PZT square tubular ultrasonic motor *Ultrasonics* **52** 880–9
[19] Roundy S, Leland E S, Baker J, Carleton E, Reilly E, Lai E, Otis B, Rabaey J M, Sundararajan V and Wright P K 2005 Improving Power Output for Vibration-Based Energy Scavengers *IEEE Pervasive Comput.* **4** 28–36
[20] Hariri H, Bernard Y and Razek A 2014 A traveling wave piezoelectric beam robot *Smart Mater. Struct.* **23** 25013
[21] Syed E M 2001 *Analysis and modeling of piezoelectric transformers*
[22] Frangi A, Corigliano A, Binci M and Faure P 2005 Finite element modelling of a rotating piezoelectric ultrasonic motor *Ultrasonics* **43** 747–55
[23] Bolborici V, Dawson F P and Pugh M C 2014 A finite volume method and experimental study of a stator of a piezoelectric traveling wave rotary ultrasonic motor *Ultrasonics* **54** 809–20
[24] Budinger M, Rouchon J-F and Nogarede B 2004 Analytical Modeling for the Design of a Piezoelectric Rotating-Mode Motor *IEEE/ASME Trans. Mechatronics* **9** 1–9
[25] Hagood N W and McFarland A J 1995 Modeling of a piezoelectric rotary ultrasonic motor *IEEE Trans. Ultrason. Ferroelectr. Freq. Control* **42** 210–24
[26] Nadal C, Pigache F and Erhart J 2015 Modeling of a ring rosen-type piezoelectric transformer by Hamilton's principle *IEEE Trans. Ultrason. Ferroelectr. Freq. Control* **62** 709–20
[27] Vasic D, Sarraute E and Costa F Dynamic 4×4 chain matrix for analytical modeling of piezoelectric actuator *2001 IEEE Ultrasonics Symposium. Proceedings. An International Symposium (Cat. No.01CH37263)* vol 2(IEEE)pp 985–8
[28] Vogel S M and Skinner D W 1965 Natural Frequencies of Transversely Vibrating Uniform Annular Plates *J. Appl. Mech.* **32** 926
[29] Martin G E 1954 Determination of Equivalent-Circuit Constants of Piezoelectric Resonators of Moderately Low *Q* by Absolute-Admittance Measurements *J. Acoust. Soc. Am.* **26** 413–20